*Fluid Dynamics & Materials Processing* FDMP, vol.15, no.3, pp.233-251, 2019

# Non-Aligned Stagnation Point Flow of a Casson Fluid Past a Stretching Sheet in a Doubly Stratified Medium

**N. Vijaya[1], G. Venkata Ramana Reddy[1, *] and Y. Hara Krishna[1]**

**Abstract:** This paper investigates the problem of oblique hydro magnetic stagnation point flow of an electrically conducting Casson fluid over stretching sheet embedded in a doubly stratified medium in the presence of thermal radiation and heat source/absorption with first order chemical reaction. It is assumed that the fluid impinges on the wall obliquely. Similarity variables were used to convert the partial differential equations to ordinary differential equations. The transformed ordinary differential equations are solved numerically using Runge-Kutta-Fehlberg method with shooting technique. It is observed that a boundary layer is formed when the stretching velocity of the surface is less than the in viscid free stream velocity at a point decreases with increase in the non-Newtonian rheology parameter. The augmentation of the temperature is observed with the magnetic parameter, heat source parameter and thermal radiation parameter while a reverse effect with thermal stratification number, Prandtl number and the velocity ratio parameter. Influence of Skin friction coefficient, Nusselt number and Sherwood number on the flow configurations for different values of pertinent parameters are portrayed graphically and discussed. Numerical results are compared with the published results and are found to be in good agreement with previously published results as special cases of present problem. The mass concentration is seen to be decrease with Schmidt number, chemical reaction parameter and solutal stratification number.

**Keywords:** Magnetic parameter, heat source, prandtl number, chemical reaction, casson fluid, free stream stagnation flow parameters.

## 1 Introduction

The study of stagnation-point flows has gained considerable attention of several researches in view of their importance in many engineering applications. These applications include rapid spray cooling and quenching in metal foundries, emergency core cooling systems, and glass blowing, etc. In some situation flow is stagnated by a solid wall, while in others a free stagnation point or line exists interior to the fluid domain. In stagnation point flow, a rigid wall or a stretching surface occupies the entire horizontal x-axis. The fluid domain is $y>0$ and the flow strikes on the stretching surface either orthogonally or at some angle of incidence. Hiemenz [Hiemenz (1911)] became first investigated the steady two-dimensional boundary-layer flow near the forward

[1] Koneru Lakshmaiah Education Foundation, Vaddeswaram, Guntur, 522502, India.

[*] Corresponding Author: G. Venkta Ramana Reddy. Email: gvrr1976@kluniversity.in.

stagnation-point on an infinite wall. Subsequently Howarth [Howrath (1935)] improved this solution. Further, various aspects of stagnation flow and heat transfer over a stretching sheet are investigated by many authors. Chiam [Chiam (1994)] analyzed the steady two-dimensional and the axisymmetric stagnation-point flow of a viscous Newtonian incompressible fluid towards a stretching surface and they observed that no boundary layer is formed, that is, the effect of the stretching plate exactly cancels the tendency to form the boundary layer. Chamkha [Chamkha (1998)] studied forced convection flow of an electrically-conducting fluid at the stagnation point of an axisymmetric body in the presence of a uniform applied magnetic field. Mahapatra et al. [Mahapatra and Gupta (2002)] investigated the heat transfer in a stagnation-point flow towards a stretching sheet. They concluded that the boundary layer is formed near the stretching surface. They observed that the structure of this boundary layer depends on the ratio of the velocity of the stretching surface to that of the frictionless potential flow in the neighborhood of the stagnation point. In a subsequent study, Gupta et al. [Gupta and Mahapatra (2003)] discussed the stagnation-point flow of an incompressible viscous fluid over a flat deformable surface when the surface is stretched axis symmetrically in its own plane with a velocity proportional to the distance from the stagnation-point. They have shown that a boundary layer is formed when the stretching velocity is less than the free stream velocity and an inverted boundary layer is formed when the stretching velocity exceeds the free stream velocity. Pop et al. [Pop, Grosan and Pop (2004)] studied the effect of thermal radiation on the stagnation point flow over a flat plate. They found that boundary layer thickness increases with radiation. Attia [Attia (2007)] studied MHD three dimensional axisymmetric stagnation point flow of an incompressible viscous fluid impinging on a permeable stretching surface with heat generation or absorption. They observed that the velocity components increase as the stretching velocity increases but velocity boundary layer thickness is seen to reduce. Zhu et al. [Zhu, Zheng and Zhang (2010)] made a study on the MHD stagnation point flow over a power-law stretching sheet considering the slip effect at the boundary. Zhu et al. [Zhu, Zheng and Zhang (2011)] analyzed the axisymmetric stagnation point flow towards a stretching sheet with velocity slip and temperature jump. They concluded that the flow and shear stresses depend heavily on the velocity slip parameter and the temperature gradient at the wall increases with velocity slip parameter and thermal slip factor. Tilley et al. [Tilley and Weidman (1998)] studied interaction between two planar oblique stagnation-point flows of different immiscible fluids. Reza et al. [Reza and Gupta (2005)] examined the steady two-dimensional oblique stagnation-point flow of a Newtonian fluid towards a stretching surface. They found that for very small shear in the free stream, the flow has a boundary layer structure and the thickness of the boundary layer decreases with increase in straining motion near the stagnation point. Further, they concluded that the flow has an inverted boundary layer structure when the stretching velocity of the surface exceeds the stagnation velocity of the free stream. In this case, the surface shear stress is found to decrease for an increase in the free-stream stagnation velocity. Lok et al. [Lok, Amin and Pop (2006)] made a numerical study of the non-orthogonal stagnation-point for Newtonian and non-Newtonian flows towards a stretching sheet. They found that the position of stagnation point depends on stretching parameter and angle of incidence. Labropulu et al. [Labropulu, Li and Pop (2010)] analyzed oblique stagnation point flow

of an incompressible visco-elastic fluid towards a stretching sheet. Rosali et al. [Rosali, Ishak and Pop (2011)] studied the stagnation point flow and heat transfer over a stretching/shrinking sheet in a porous medium. They showed that dual solutions exist for the shrinking case. Nadeem et al. [Nadeem and Lee (2012)] performed a numerical investigation of the non-orthogonal stagnation point flow of a non-Newtonian nanofluid towards a stretching surface and concluded that heat transfer decreases with an increase in Brownian motion and thermo-phoresis parameters. Nadeem et al. [Nadeem, Rashid Mehmood and Noreen Sher Akbar (2015)] studied the partial slip effect on the non-orthogonal stagnation point nanofluid over a convective stretching surface. Khan et al. [Khan, Makinde and Khan (2016)] studied the effect of variable viscosity on the non-aligned hydromagnetic stagnation point flow of an electrically conducting viscous incompressible nanofluid over a convectively heated stretching sheet taking into account of the thermal radiation. They observed that non-alignment of the re-attachment point on the sheet surface decreases with an increase in magnetic field intensity. Mustafa et al. [Mustafa, Mushtaq, Hayat et al. (2016)] examined MHD non-aligned stagnation point flow of an upper convicted Maxwell fluid over a continuously deforming surface under the influence on non-linear thermal radiation. Mehmood et al. [Mehmood, Nadeem and Sher Akbar (2016)] analyzed the non-aligned stagnation point flow and heat transfer of a Nano fluid towards a stretching surface. Zaffar et al. [Zaffar, Mehmood and Iqbal (2017)] investigated numerical solution of micropolar Casson fluid over a stretching sheet with internal heating. Rana et al. [Rana, Rashid Mehmood and Noreen Sher (2016)] analyzed mixed convective oblique flow of a Casson fluid with partial slip, internal heating and homogeneous-heterogeneous reactions. Iqbal et al. [Iqbal, Mehmood, Ehtsham et al. (2017)] explored the Impact of inclined magnetic field on micropolar Casson fluid using Keller box algorithm. Tabassum et al. [Tabassum, Mehmood and Nadeem (2017)] studied impact of viscosity variation and micro rotation on oblique transport of cu-water fluid. Nadeema et al. [Nadeema, Rashid Mehmood and Masooda (2016)] identified the effects of transverse magnetic field on a rotating micro polar fluid between parallel plates with heat transfer. Rehmana et al. [Aziz Ur Rehmana, Rashid Mehmood, Nadeem et al. (2017)] analyzed Entropy of radioactive rotating nanofluid with thermal slip. Ganesh Kumar et al. [Ganesh Kumar, Gireesha and Gorla (2018)] studied flow and heat transfer of dusty hyperbolic tangent fluid over a stretching sheet in the presence of thermal radiation and magnetic field. Ganesh Kumar et al. [Ganesh Kumar, Gireesha, Manjunatha et al. (2017)] explored the effect of nonlinear thermal radiation on double-diffusive mixed convection boundary layer flow of viscoelastic nanofluid over a stretching sheet. Ganesh Kumar et al. [Ganesh Kumar, Rudraswamy, Gireesha et al. (2017)] performed the experiment to find effects of mass transfer on MHD three dimensional flow of a Prandtl liquid over a flat plate in the presence of chemical reaction. Ganesh Kumar et al. [Ganesh Kumar, Gireesha, Prasannakumara et al. (2017)] studied phenomenon of radiation and viscous dissipation on Casson nano liquid flow past a moving melting surface. Eldabe et al. [Eldabe and Salwa (1995)] studied heat transfer of MHD non-Newtonian Casson fluid flow between two rotating cylinders. Labropulu et al. [Labropulu, Li and Pop (2010)] analysed Non-orthogonal stagnation-point flow towards a stretching surface in a non-Newtonian fluid with heat transfer. Nadeem et al. [Nadeem, Mehmood and Akbar (2013)] explored Non-orthogonal stagnation point flow of a nano non-Newtonian fluid towards a

stretching surface with heat transfer. Khan et al. [Khan, Makinde and Khan (2016)] studied Non-aligned MHD stagnation point flow of variable viscosity nanofluid past a stretching sheet with radiative heat.

## 2 Mathematical formulation

We consider the two dimensional incompressible boundary layer flow of a Casson fluid over a stretching sheet located at $y = 0$ (see Fig. 1). The sheet is stretched through two equal and opposite forces along x-axis by keeping the origin fixed with the velocity $u_w = bx$, b is a positive constant with dimension per time. Let $u_e = ax + cy$ be the fluid's velocity outside the boundary layer, where $a$ and $c$ are positive constants with dimension per time.

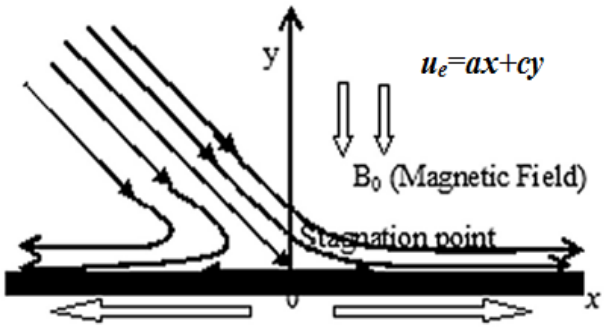


**Figure 1:** Physical model and coordinate system

The surface has temperature $T_w$ and concentration $C_w$ and further $T_\infty$ and $C_\infty$ are respectively the temperature and concentration of the ambient fluid. Thermal and concentration stratifications are taken into account in the presence of thermal radiation and heat source/sink. A uniform magnetic field of strength $B_0$ is assumed to be applied normal to the stretching surface. The magnetic Reynolds number is taken to be small and therefore the induced magnetic field and electric field are neglected.

The constitutive equation of the isotropic and incompressible Casson fluid can be written as [Eldabe and Salwa (1995)]:

$$\tau_{ij} = \begin{cases} 2\left(\mu_B + \frac{P_y}{\sqrt{2\pi}}\right) e_{ij}, & \pi > \pi_c, \\ 2\left(\mu_B + \frac{P_y}{\sqrt{2\pi_c}}\right) e_{ij}, & \pi < \pi_c \end{cases} \tag{1}$$

where $\tau_{ij}$ is the (i, j):th component of the stress tensor, $\mu_B$ is the plastic dynamic viscosity of the non-Newtonian fluid, $P_y$ is the yield stress of the fluid, $\pi$ is the product of the component of deformation rate with itself, namely, $\pi = e_{ij}e_{ij}$, and $e_{ij}$ is the (i, j):th component of deformation rate, and $\pi_c$ is critical value of $\pi$ based on the non-Newtonian model. Therefore, when the shear stress is smaller than the yield stress $P_y$, the fluid exhibits no motion, i.e., it behaves like a solid, but when the shear stress is greater than $P_y$, it demonstrates flow characteristics.

The governing partial differential equations under boundary layer assumptions of the flow are given below:

$$\frac{\partial u}{\partial x} + \frac{\partial v}{\partial y} = 0 \tag{2}$$

$$u\frac{\partial u}{\partial x} + v\frac{\partial u}{\partial y} = \nu\left(1+\frac{1}{\beta}\right)\frac{\partial^2 u}{\partial y^2} + u_e\frac{\partial u_e}{\partial x} - \frac{\sigma B_0^2}{\rho}(u-u_e) \tag{3}$$

$$u\frac{\partial T}{\partial x} + v\frac{\partial T}{\partial y} = \frac{k}{\rho c_p}\frac{\partial^2 T}{\partial y^2} + \frac{16\sigma^* T_\infty^3}{3k^*\rho c_p}\frac{\partial^2 T}{\partial y^2} + \frac{\mathrm{Q}_0}{\rho c_p}(\mathrm{T}-T_\infty) \tag{4}$$

$$u\frac{\partial C}{\partial x} + v\frac{\partial C}{\partial y} = D\frac{\partial^2 C}{\partial y^2} - k_0(C-C_\infty) \tag{5}$$

where u and v are fluid velocity components along $x$ and $y$-axes, respectively, $\nu$ is kinematic viscosity,

$\beta = \mu_B\sqrt{2\pi_c}/P_y$ is the Casson parameter, $\rho$ is density of the fluid, $\sigma$ is electrical conductivity, $T$ is fluid temperature, $C$ is fluid concentration, $k$ is thermal conductivity of the fluid, $c_p$ is specific heat at constant pressure, $\sigma^*$ is Stefen-Boltzman constant, $k^*$ is absorption coefficient, $\mathrm{Q}_0$ is heat generation ($\mathrm{Q}_0 > 0$) or absorption ($\mathrm{Q}_0 < 0$) coefficient, D is mass diffusivity and $k_0$ is the chemical reaction.

The appropriate boundary conditions for the problem are

$$u = u_w,\ v = 0,\ T = T_w = T_0 + m_1 x,\ C = C_w = C_0 + n_1 x \text{ at } y = 0 \tag{6}$$

$$u \to u_e,\quad T \to T_\infty = T_0 + m_2 x,\quad C \to C_\infty C_0 + n_2 x \text{ as } y \to \infty \tag{7}$$

where $m_1, m_2, n_1, n_2$ are dimensional constants and $T_0$, $C_0$ are the reference temperature and reference concentration, respectively.

## 3 Method of solution

Equations and mathematical expressions must be inserted into the main text. Two different types of styles can be used for equations and mathematical expressions. They are: in-line style, and display style.

The governing partial differential Eqs. (3)-(5) can be reduced to a set of ordinary differential equations by introducing the following similarity variables

$$\eta = \sqrt{b/\nu}\ y,\quad X = \sqrt{b/\nu}\ x \tag{8}$$

From the continuity Eq. (1), we can define the stream function

$$\psi(X,\eta) = \nu[Xf(\eta) + g(\eta)] \tag{9}$$

where, $f(\eta)$ and $g(\eta)$ represent the normal and tangential components of flow respectively, such that

$$u = \sqrt{\frac{b}{\nu}}\frac{\partial \psi}{\partial \eta}, \qquad v = -\sqrt{\frac{b}{\nu}}\frac{\partial \psi}{\partial X} \tag{10}$$

which automatically satisfy the continuity Eq. (1):

$$u = \sqrt{b\nu}(Xf'(\eta) + g'(\eta)), \qquad v = -\sqrt{b\nu}f(\eta),\quad \theta(\eta) = \frac{T-T_\infty}{T_w-T_0}, \phi(\eta) = \frac{C-C_\infty}{C_w-C_0} \tag{11}$$

Substituting Eq. (10): into (3): - (5):, we obtain

$$\left(1+\frac{1}{\beta}\right)f''' + ff'' - f'^2 - M(f'-A) + A^2 = 0 \tag{12}$$

$$\left(1+\frac{1}{\beta}\right)g'''+fg''-f'g'-M(g'-B\eta)+RB=0 \quad (13)$$

$$\left(1+\frac{4}{3}Nr\right)\theta''+Pr(f\theta'-f'\theta-\varepsilon_1 f'+Q\theta)=0 \quad (14)$$

$$\phi''+Sc(f\phi'-f'\phi-\varepsilon_2 f'-\gamma\phi)=0 \quad (15)$$

The associated boundary conditions are

$$f(0)=0, f'(0)=1, g'(0)=0,\ \theta(0)=1-\varepsilon_1,\ \phi(0)=1-\varepsilon_2 \quad (16)$$

$$f'(\infty)\to A,\ g''(\infty)\to B, \theta(\infty)\to 0,\ \phi(\infty)\to 0 \quad (17)$$

From Eq. (17), it can be easily seen that $f(\eta)=A\,\eta+R$ as$\eta\to\infty$, where R is the boundary layer displacement constant to be determined.

Let$g'(\eta)=B\,G(\eta)$ (18)

Substituting Eq. (18) into Eq. (13) we obtain

$$\left(1+\frac{1}{\beta}\right)G''+fG'-Gf'-M(G-\eta)+R=0 \quad (19)$$

$$f(0)=0, f'(0)=1, G(0)=0,\ \theta(0)=1-\varepsilon_1,\ \phi(0)=1-\varepsilon_2 \quad (20)$$

$$f'(\infty)\to A,\ G'(\infty)\to 1, \theta(\infty)\to 0,\ \phi(\infty)\to 0 \quad (21)$$

where,

$M=\frac{\sigma B_0^2}{\rho b}$ (Magnetic field parameter):

$A=\frac{a}{b}; B=\frac{c}{b}$ (Free stream stagnation flow parameters):

$Pr=\frac{\rho c_p \nu}{k}$ (Prandtl number):

$Nr=\frac{4\sigma^* T_\infty^3}{kk^*}$ (Thermal radiation parameter):

$Q=\frac{Q_0}{\rho c_p b}$ (Heat source/sink parameter):

$Sc=\frac{\nu}{D}$ (Schmidt number):

$\varepsilon_1=\frac{m_2}{m_1}$ (Thermally stratified parameter):

$\varepsilon_2=\frac{n_2}{n_1}$ (Solutal stratified parameter):

$\gamma=\frac{k_0}{b}$ (Chemical reaction parameter)

The surface skin friction coefficient $C_f$, local Nusselt number $Nu$ and local Sherwood number $Sh$ which have a significant role in engineering and are defined by

$$C_f=\frac{\tau_w}{\rho u_e^2},\ Nu=\frac{xq_w}{k(T_w-T_\infty)},\ Sh=\frac{xm_w}{D(C_w-C_\infty)} \quad (22)$$

where the wall shear stress $\tau_w$, the surface heat flux $q_w$ and mass flux $m_w$ are given by

$$\tau_w=\mu\left(1+\frac{1}{\beta}\right)\left(\frac{\partial u}{\partial y}\right)_{y=0},\quad q_w=-k\left(1+\frac{16\sigma^* T^3}{3kk^*}\right)\left(\frac{\partial T}{\partial y}\right)_{y=0}, m_w=-D\left(\frac{\partial C}{\partial y}\right)_{y=0}, \quad (23)$$

and μ is dynamic viscosity of the fluid.

Using Eq. (23) in Eq. (22), we obtain

$$C_f = \left(1 + \frac{1}{\beta}\right)\left(Xf''(0) + BG'(0)\right)$$

$$Nu = -\left(1 + \frac{4}{3}Nr\right)\theta'(0)$$

$$Sh = -\phi'(0)$$

The ordinary differential Eqs. (12), (14), (15) and (19) are coupled and highly non-linear. These equations with the boundary conditions (20) and (21) are solved using Runge-Kutta-Fehlberg method with shooting technique and obtained numerical solutions. The numerical scheme is validated by comparing the values of $f''(0)$ and $G'(0)$ of the investigation under discussion with those calculated by Labropulu et al. [Labropulu, Li and Pop (2010); Nadeem, Rashid Mehmood and Noreen Sher Akbar (2015); Khan, Makinde and Khan (2016)] in the absence of magnetic field and for the case of a Newtonian fluid for different values of A.

## 4 Results and discussion

The influence of free stream stagnation flow parameter A for fixed values of 'b' on flow pattern is depicted in the Fig. 2. When A>1 straining motion in the neighborhood of the stagnation point increases. As a result, the external stream velocity accelerates and increases boundary layer thickness. This physical phenomena is the reason for boundary layer structure of the fluid motion. When $A < 1$, the flow has an inverted boundary layer structure. This arises from the fact that when $A < 1$, the stretching velocity of the surfaces exceeds the stagnation velocity of the external stream. The oblique velocity profiles for different values in Fig. 3. It is clearly seen from Fig. 4 that the non-dimensional temperature decreases for an increase in A with a reduction in the thickness of the thermal boundary layer. The variation of the stretching parameter on concentration is illustrated in Fig. 5. It is observed that concentration distribution is a decreasing function of the stretching ratio.

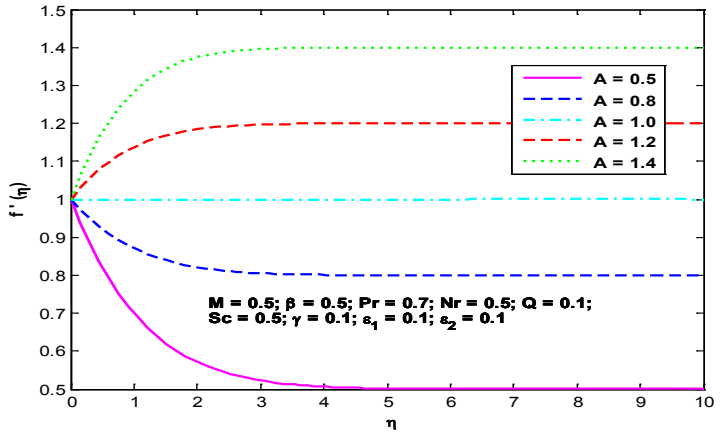


**Figure 2:** Axial velocity profiles for different values A

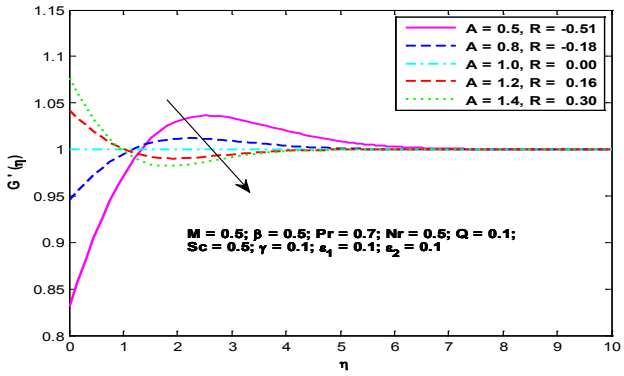


**Figure 3:** Obliquevelocity gradient profiles for different values of A

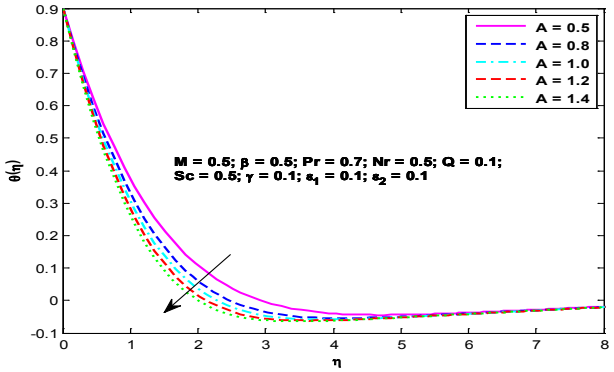


**Figure 4:** Temperature profiles for different values of A

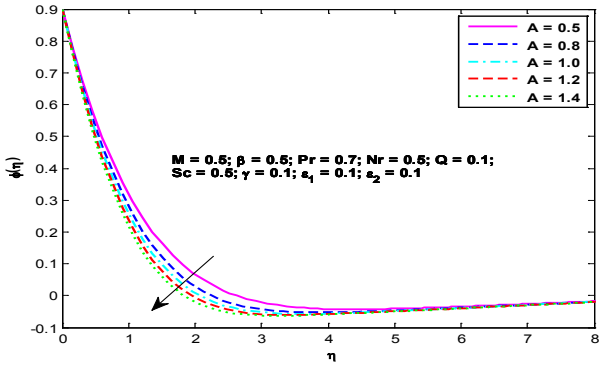


**Figure 5:** Concentration profiles for different values of A

The effect of Casson parameter $\beta$on axial velocity profiles is portrayed in Fig. 6. Axial velocity diminishes with increased values of $\beta$. It is observed from Fig. 7 that oblique velocity gradient is to enhance with increasing $\beta$ in the vicinity of the boundary in the region $0 \leq \eta \leq 2.929$ and later it shows a reverse trend in the region $2.929 \leq \eta \leq 8.687$, and after that it is steady. Fig. 8 & Fig. 9 are the plots of temperature and species

concentration for a variation of Casson parameter. It is seen that temperature and concentration are increasing functions of $\beta$.

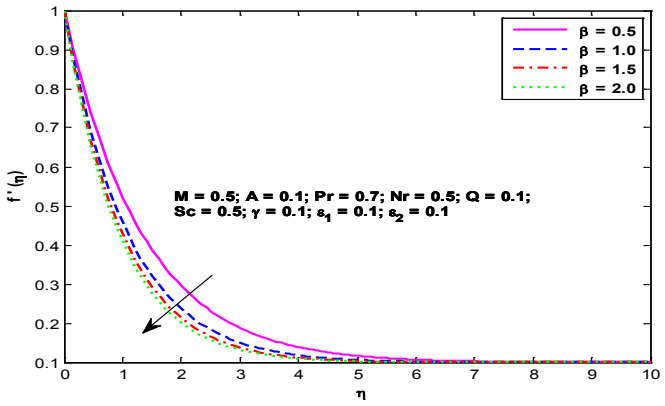


**Figure 6:** Axial velocity profiles for different values $\beta$

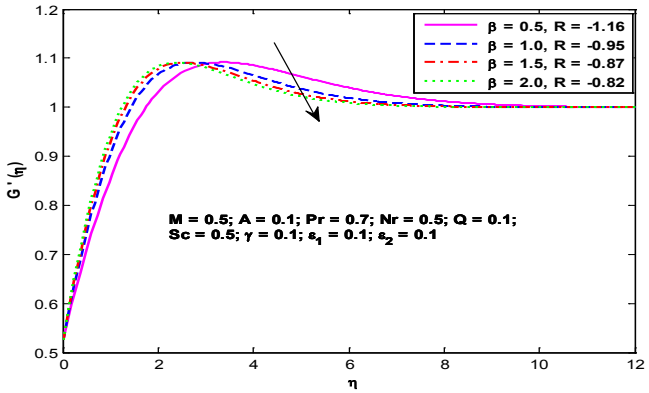


**Figure 7:** Obliquevelocity gradient profiles fordifferent values of $\beta$

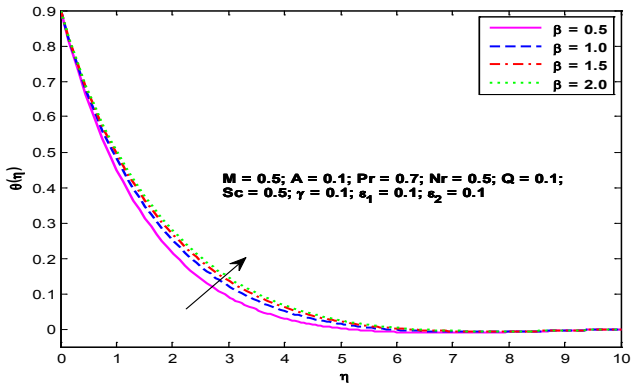


**Figure 8:** Temperature profiles for different values of $\beta$

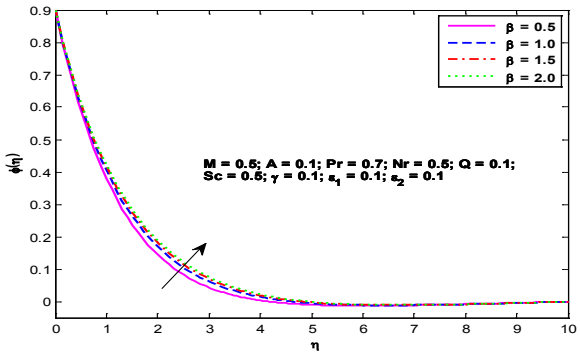


**Figure 9:** Concentration profiles for different values of $\beta$

The axial velocity diminishes with increase in magnetic field M strength as shown in Fig. 10. This is in conformity of the fact that the stronger Lorentz force generated as a result of application of M opposes the fluid motion. From Fig. 11, it is found that as $M$ takes higher values the oblique velocity gradient $G'(\eta)$ increases near the wall and subsequently it reduces. Fig. 12 shows that increase in the magnetic field strength facilitates the augmentation of temperature distribution. Thus the thickness of the thermal boundary layer enhances. The effect of M on concentration is seen to be the same as that on temperature and this can be observed from Fig. 13.

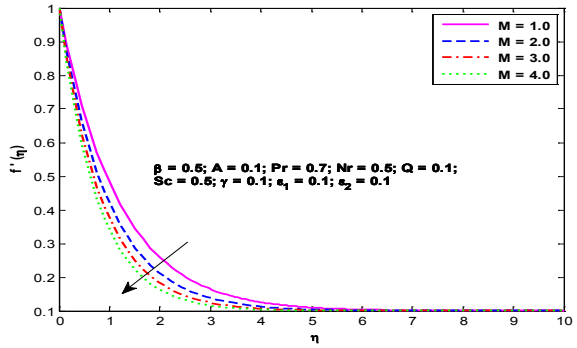


**Figure 10:** Axial velocity profiles for different values M

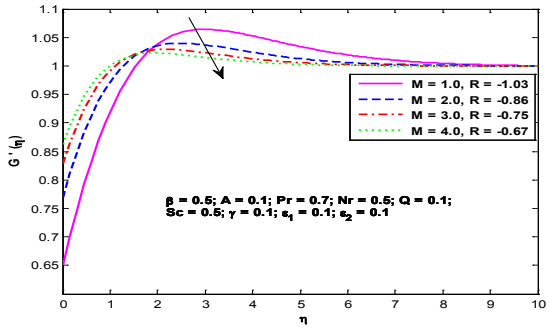


**Figure 11:** Obliquevelocity gradient profiles for different values of M

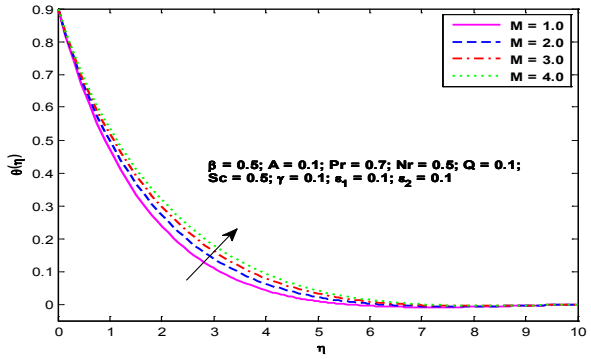


**Figure 12:** Temperature profiles for different values of M

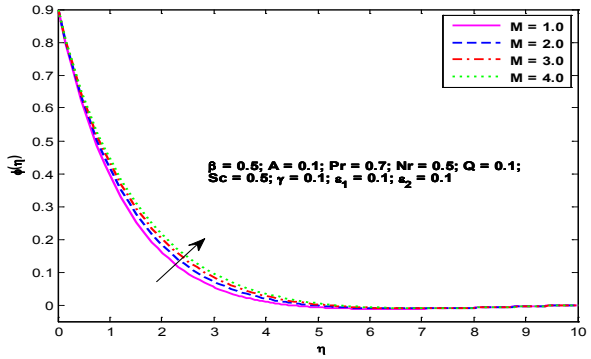


**Figure 13:** Concentration profiles for different values of M

It is evident from Fig. 14 that higher values of Prandtl number (Pr) tend to decrease the temperature due to the lower thermal conductivity of the fluid. Fig. 15 shows that the temperature is enhanced significantly for increasing values of thermal radiation parameter Nr as thermal radiation facilitates more heat to the fluid leading to an increase in the energy transport to the fluid. The associated thermal boundary layers become thicker for increasing values of Nr.

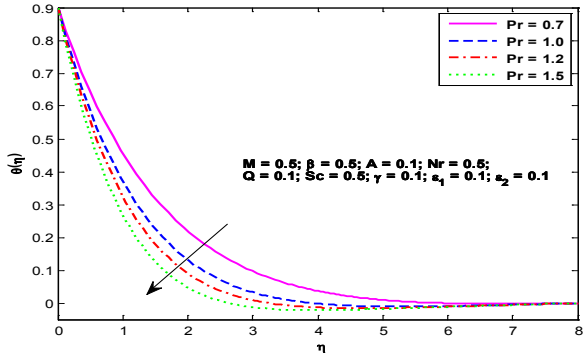


**Figure 14:** Temperature profiles for different values of Pr

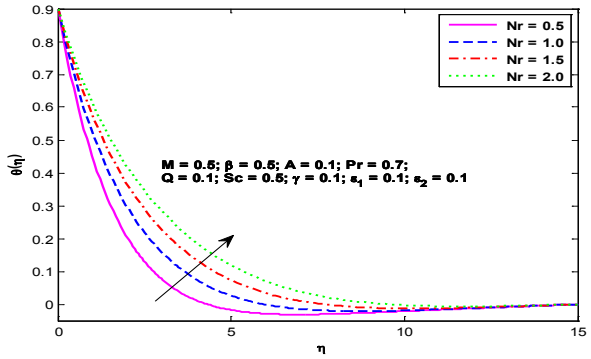


**Figure15:** Temperature profiles for different values of Nr

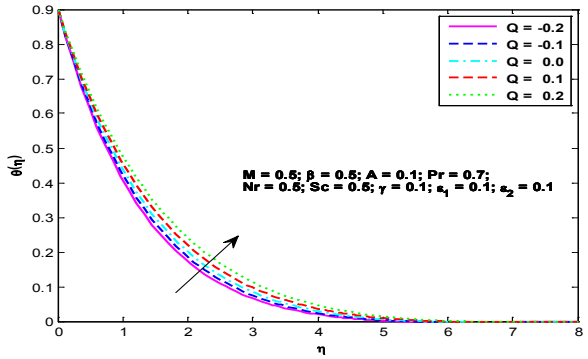


**Figure 16:** Temperature profiles for different values of Q

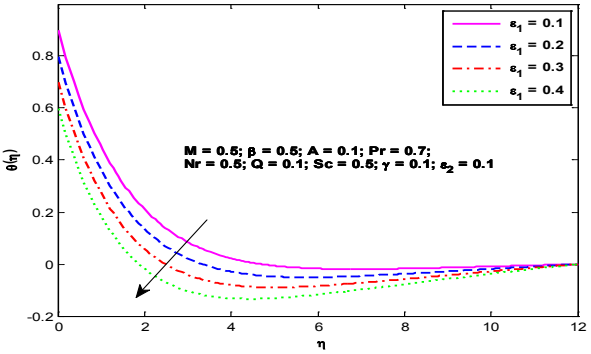


**Figure 17:** Temperature profiles for different values of $\varepsilon_1$

Fig. 16 portrays the influence of heat source/sink parameter Q on temperature distribution. Temperature profile shows a decreasing pattern with $\eta$ in the region $0 \leq \eta \leq 6$ and outside the region it tends to attain the free stream temperature. The effect of thermal stratification parameter $\varepsilon_1$ on temperature is portrayed in Fig. 17. It is observed that for small values of $\varepsilon_1$, temperature decreases steadily along $\eta$ near the surface and away from the surface there is a significant reduction in the region $1.5 \leq \eta \leq 3$ and outside this

region temperature steadily increases and eventually approaches the free stream value. Further increasing values of $\varepsilon_1$ have a reducing influence on temperature.

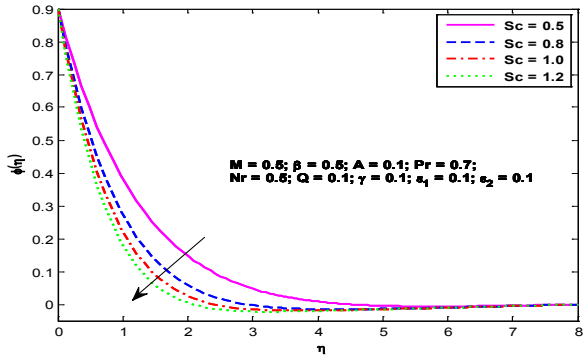


**Figure 18:** Concentration profiles for different values of Sc

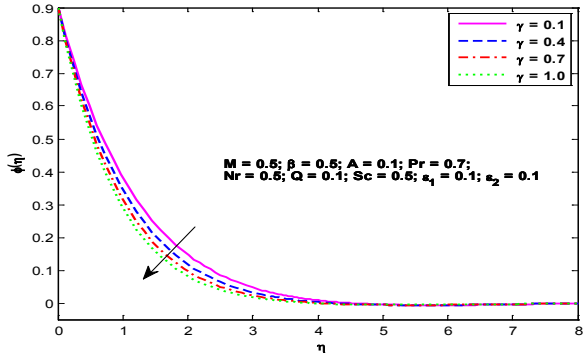


**Figure 19:** Concentration profiles for different values of $\gamma$

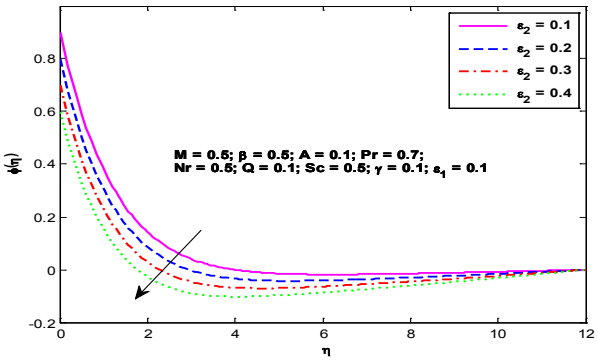


**Figure 20:** Concentration profiles for different values of $\varepsilon_2$

Influence of Schmidt number Sc on species concentration is seen to reduce species it significantly for increasing values of Sc as illustrated in Fig. 18. From Fig. 19, it is observed that for a fixed value of chemical reaction parameter $\gamma$ species concentration decreases along $\eta$ in the region $0 \leq \eta \leq 5$ and is seen to be a decreasing function of

chemical reaction parameter. Effect of solutal stratification parameter $\varepsilon_2$ is seen only on species concentration and it can be seen from Fig. 20 that species concentration decreases with increasing values of $\varepsilon_2$.

From Fig. 21, it is seen that the normal component of skin friction coefficient on the wall decreases with increase in Casson parameter as well as magnetic field parameter. The combined effect of Casson parameter and magnetic field is to decrease skin friction coefficient predominantly. It is observed that reduction in the skin friction coefficient when $M = 4.0, \beta = 1.0$ is almost fourfold to that of the case when $M = 1$ and$\beta = 0.1$.

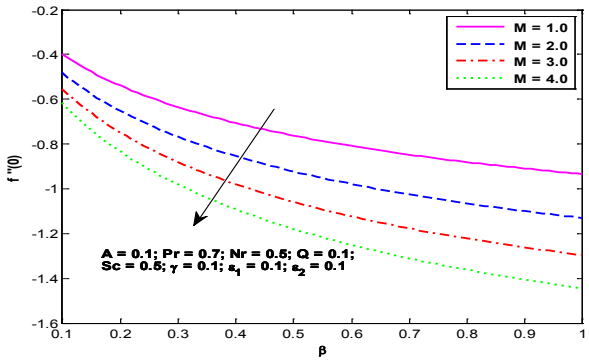


**Figure 21:** Variation of normal component of skin friction coefficient with $\beta$ for different values of M

The local Nusselt number versus velocity ratio parameter A for different values of Prandtl number is plotted in Fig. 22. It is found that Nusselt number increases almost linearly with A. Increasing values of Prandtl number also enhance Nusselt number. Variation of thermal stratification parameter and thermal radiation parameter on Nusselt number is plotted in Fig. 23. Nusselt number is seen to be a decreasing function of $\varepsilon_1$ and Nr when $Nr = 0.5$ as $\varepsilon_1$ changes from 0.1 to 1.0 the Nusselt number reduces in the range 0.6 to 0.55. For the same range of $\varepsilon_1$, when $Nr = 2.0$, the Nusselt number reduces in the range 0.36 to 0.26. Fig. 24 shows the plot of Sherwood number versus solutal stratification number for a variation of Schmidt number. It is seen that the Sherwood number reduces with increase in $\varepsilon_2$ while it increases as Schmidt number increases.

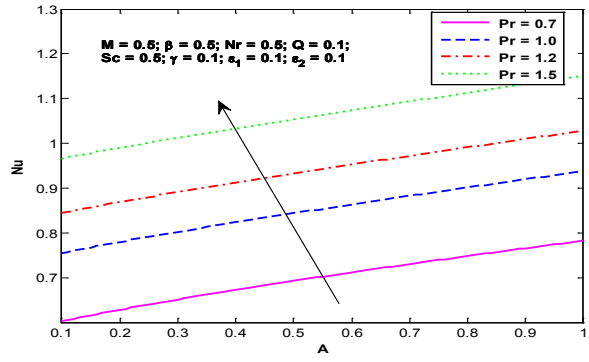


**Figure 22:** Variation of Nusselt number with Afor different values of Pr

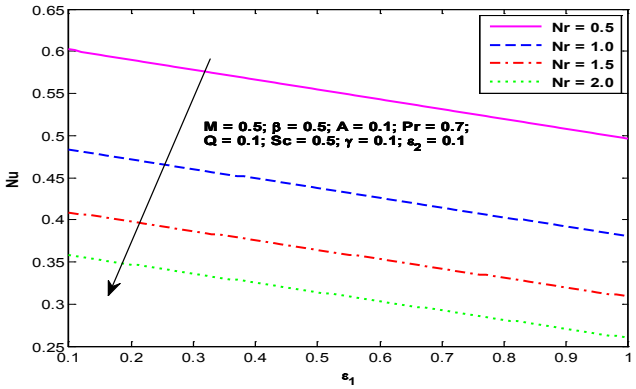


**Figure 23:** Variation of Nusselt number with $\varepsilon_1$ for different values of Nr

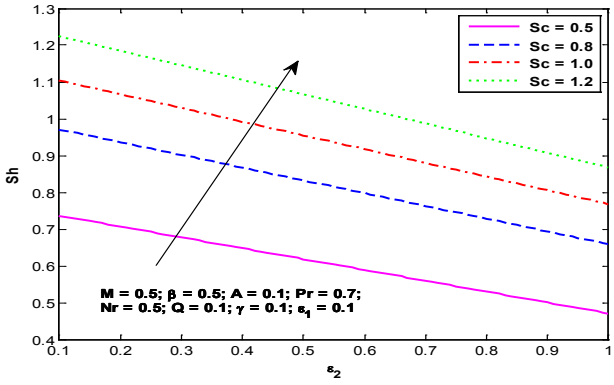


**Figure 24:** Variation of Sherwood number with $\varepsilon_2$ for different values of Sc

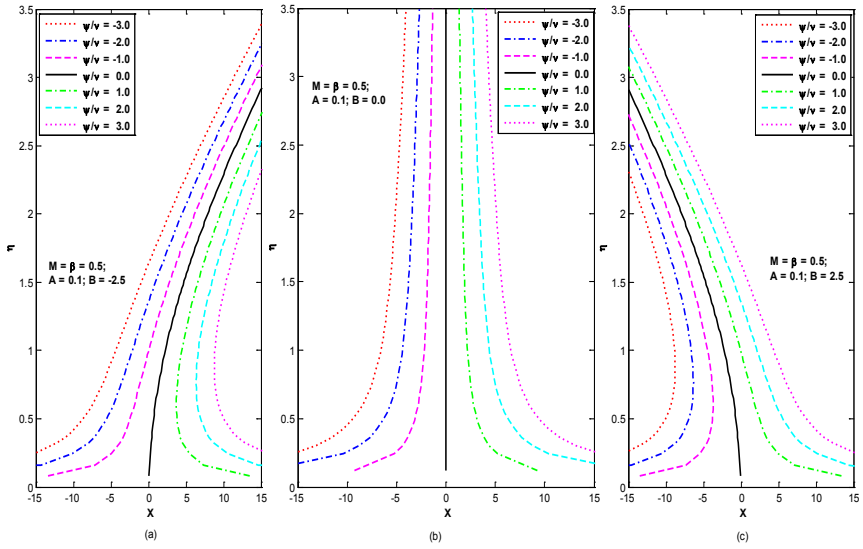


**Figure 25:** Streamline patterns for the oblique flow. (a) non-aligned pattern for $\boldsymbol{B = -2.5}$; (b) aligned pattern for $\boldsymbol{B = 0}$; (c) non-aligned pattern for $\boldsymbol{B = 2.5}$

The streamlines of the flow for different values of B are illustrated in Fig. 25. For $B < 0$ the streamlines are skewed towards right of the stagnation point and towards left for $B > 0$ as expected and when $B = 0$ the streamlines are seen to be normal to the surface. Fig. 26 shows that the stream lines are more and more skewed towards the right (left) of the stagnation point for an increase in $B > 0$ ($B < 0$) due to the increase in the straining motion.

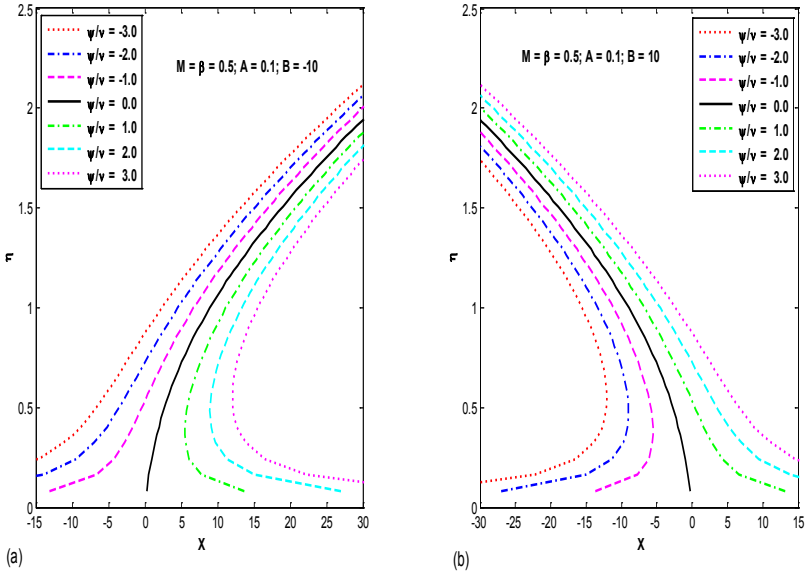


**Figure 26:** Streamline patterns for oblique flow. (a) non-aligned pattern for $\boldsymbol{B = -10}$; (b) Non-aligned pattern for $\boldsymbol{B = 10}$

Tab. 1 shows the comparison of present results with that of previous results of Labropulu et al. [Labropulu, Li and Pop (2010); Nadeem, Rashid Mehmood and Noreen Sher Akbar (2015); Khan, Makinde and Khan (2016)].

**Table 1:** Comparison values of $f''(0)$ and $'(0)$ for various values of A when $M = 0, \beta \to \infty$

| A | R | Labropulu, Li and Pop (2010) | | Nadeem, Rashid Mehmood and Noreen Sher Akbar (2015) | | Khan, Makinde and Khan (2016) | | Present Results | |
|---|---|---|---|---|---|---|---|---|---|
| | | $f''(0)$ | $G'(0)$ | $f''(0)$ | $G'(0)$ | $f''(0)$ | $G'(0)$ | $f''(0)$ | $G'(0)$ |
| 0.1 | -0.791705 | -0.96938 | 0.26278 | -0.96938 | 0.26332 | -0.969386 | 0.26332 | -0.96938 | 0.26332 |
| 0.3 | -0.519499 | -0.84942 | 0.60573 | -0.84942 | 0.60631 | -0.849420 | 0.60631 | -0.84942 | 0.60631 |
| 0.8 | | | 0.93430 | | 0.93472 | | 0.93472 | | 0.93472 |
| 2.0 | -0.114527 | -0.29938 | 1.16489 | -0.29938 | 1.16521 | -0.299388 | 1.16521 | -0.29938 | 1.16521 |
| 3.0 | 0.410407 | 2.01750 | 1.23438 | 2.01750 | 1.23465 | 2.017502 | 1.23465 | 2.01750 | 1.23465 |
| | 0.693053 | 4.72928 | | 4.72928 | | 4.729282 | | 4.72928 | |

## 5 Conclusions

Non-aligned hydro magnetic stagnation point flow of a Casson fluid over a stretching surface in a doubly stratified medium with radioactive heat source and internal heat generation has been analyzed numerically. The results of this analysis can be summarized as follows:

- Combined effect of Casson parameter and magnetic field is to reduce velocities heavily.
- Velocity ratio parameter decreases the temperature and concentration.
- Boundary layer thickness is reduced by velocity ratio parameter.
- The non-dimensional temperature distribution is enhanced by thermal radiation while the thermal stratification parameter has a reducing influence on temperature.
- The dimensionless concentration decreases with Schmidt number, solutal stratification parameter and chemical reaction parameter.
- The normal component of skin friction decreases with magnetic field as well as Casson parameter.
- Nusselt number increase with Prandtl number and velocity ratio parameter.
- Schmidt number tends to increase Sherwood number while solutal stratification parameter decreases the same.
- Streamlines are oblique towards the left of the stagnation point for $B > 0$ as a result of straining motion and a reversal trend is noticed for $B < 0$.

## References

**Attia, H. A.** (2007): Axisymmetric stagnation point flow towards a stretching surface in the presence of a uniform magnetic field with heat generation. *Tamkang Journal of Scence and Engineering*, vol. 10, no. 1, pp. 11-16.

**Chamkha, A. J.** (1998): Hydromagnetic plane and axisymmetric flow near a stagnation point with heat generation. *International Communication of Heat Mass Transfer*, vol. 25, no. 2, pp. 269-278.

**Chiam, T. C.** (1994): Stagnation-point flow towards a stretching plate. *Journal of the Physical Society of Japan*, vol. 63, pp. 2443-2444.

**Eldabe, N. T. M.; Salwa, M. G. E.** (1995): Heat transfer of MHD non-Newtonian Casson fluid flow between two rotating cylinders. *Journal of the Physical Society of Japan*, vol. 64, 41.

**Ganesh Kumar, K.; Gireesha, B. J.; Manjunatha, S.; Rudraswamy, N. G.** (2017): Effect of nonlinear thermal radiation on double-diffusive mixed convection boundary layer flow of viscoelastic nanofluid over a stretching sheet. *International Journal of Mechanical and Materials Engineering*.

https://link.springer.com/article/10.1186%2Fs40712-017-0083-5.

**Ganesh Kumar, K.; Gireesha, B. J.; Gorla, R, S. R.** (2018): Flow and heat transfer of dusty hyperbolic tangent fluid over a stretching sheet in the presence of thermal radiation and magnetic field. *International Journal of Mechanical and Materials Engineering*, vol. 13, no. 2, pp. 1-11.

**Ganesh Kumar, K.; Gireesha, B. J.; Prasannakumara, B. C.; Ramesh, G. K.; Makinde, O. D.** (2017): Phenomenon of radiation and viscous dissipation on Casson nanoliquid flow past a moving melting surface. *Diffusion Foundations*, vol. 11, pp. 33-42.

**Gupta, A. S.; Mahapatra, T. R.** (2003): Stagnation point flow towards a stretching surface. *Canadian Journal of Chemical Engineering*, vol. 81, pp. 258-263.

**Hiemenz, K.** (1911): Die Grenzschicht an einem in den gleichförmingen Flussigkeitsstrom eingetauchten geraden Kreiszylinder. *Dinglers Polytech Journal*, vol. 326, pp. 321-410.

**Howrath, L.** (1935): On the calculation of the steady flow in the boundary layer near the surface of a cylinder in a stream. *ARCRM*, pp. 1632.

**Iqbal, Z.; Mehmood, R.; Azhar, E.; Mehmood, Z. (**2017): Impact of inclined magnetic field on micropolar Casson fluid using Keller box algorithm. *Physics Journal Plus*, vol. 132, pp. 175.

**Khan, W. A.; Makinde, O. D.; Khan, Z. H.** (2016): Non-aligned MHD stagnation point flow of variable viscosity nanofluids past a stretching sheet with radiative heat. *International Journal of Heat and Mass Transfer*, vol. 96, pp. 525-534

**Khan, W. A.; Makinde, O. D.; Khan, Z. H.** (2016): Non-aligned MHD stagnation point flow of variable viscosity nanofluids past a stretching sheet with radiative heat. *International Journal of Heat and Mass Transfer*, vol. 96, pp. 525-534.

**Kumar, K. G.; Rudraswamy, N. G.; Gireesha, B. J.** (2017) Effects of mass transfer on MHD three dimensional flow of a Prandtl liquid over a flat plate in the presence of chemical reaction. *Results in Physics*, vol. 7, pp. 3465-3471.

**Labropulu, F.; Li, D.; Pop, I.** (2010): Non-orthogonal stagnation-point flow towards a stretching surface in a non-Newtonian fluid with heat transfer. *International Journal Thermal Sciences*, vol. 49, pp. 1042-1050.

**Lok, Y. Y.; Amin, N.; Pop, I.** (2006): Nonorthogonal stagnation point flow towards a stretching sheet. *International Journal of Non-Linear Mechanics*, vol. 41, pp. 622-627

**Mahapatra, T. R.; Gupta, A. S.** (2002): Heat transfer in stagnation-point flow towards a stretching sheet. *Heat and Mass Transfer*, vol. 38, pp. 517-521.

**Mehmood, R.; Nadeem, S.; Akbar, N. S.** (2016): Non-aligned ethylene-glycol 30% based stagnation point fluid over a stretching surface with hematite nano particles. *Journal of Applied Fluid Mechanics*, vol. 9, no. 3, pp. 1359-1366.

**Mehmood, Z.; Mehmood, R.; Iqbal, Z.** (2017): Numerical investigation of micropolar casson fluid over a stretching sheet with internal. *Communications in Theoretical Physics*, vol. 67, no. 4, pp. 443.

**Mustafa, M.; Mushtaq, A.; Hayat, T.; Alsaedi, A.** (2016): Non-aligned MHD stagnation-point flow of upper-convected Maxwell fluid with nonlinear thermal radiation. *Neural Computing & Applications*.

**Nadeem, S.; Lee, C.** (2012): Boundary layer flow of nanofluid over an exponentially stretching sheet. *Nanoscale Research Letters*, vol. 91, pp. 1-6.

**Nadeem, S.; Mehmood, R.; Akbar, N. S.** (2013): Non-orthogonal stagnation point flow of a nano non-Newtonian fluid towards a stretching surface with heat transfer. *International Journal Heat Mass Transfer*, vol. 57, no. 2, pp. 679-689.

**Nadeem, S.; Mehmood, R.; Akbar, N. S.** (2015): Partial slip effect on non-aligned stagnation point nanofluid over a stretching convective surface. *Chinese Journal of Physics B*, vol. 24, no. 1, pp. 1-8.

**Nadeema, S.; Mehmood, R.; Masooda, S.** (2016): Effects of transverse magnetic field on a rotating micropolar fluid between parallel plates with heat transfer. *Journal of Magnetism and Magnetic Materials*, vol. 401, pp. 1006-1014.

**Pop, S. R.; Grosan, T.; Pop, I.** (2004): Radiation effects on the flow near the stagnation point of a stretching sheet. *Technische Mechanik*, vol. 25, pp. 100-106.

**Rana, S.; Mehmood, R.; Akbar, N. S.** (2016): Mixed convective oblique flow of a Casson fluid with partial slip, internal heating and homogeneous–heterogeneous reactions. *Journal of Molecular Liquids*, vol. 222, pp. 1010-1019

**Rehman, A. U.; Mehmood, R.; Nadeem, S.** (2017): Entropy analysis of radioactive rotating nanofluid with thermal slip. *Applied Thermal Engineering*, vol. 112, pp. 832-840.

**Reza, M.; Gupta, A. S.** (2005): Steady two-dimensional oblique stagnation-point flow towards a stretching surface. *Fluid Dynamics Research*, vol. 37, pp. 334-340.

**Rosali, H.; Ishak, A.; Pop, I.** (2011): Stagnation point flow and heat transfer over a stretching/shrinking sheet in a porous medium. *International Communications in Heat and Mass Transfer*, vol. 38, pp. 1029-1032.

**Tabassum, R.; Mehmood, R.; Nadeem S.** (2017): Impact of viscosity variation and micro rotation on oblique transport of Cu-water fluid. *Journal of Colloid and Interface Science*, vol. 501, pp. 304-310.

**Tilley, B. S.; Weidman, P. D.** (1998): Oblique two-fluid stagnation-point flow. *European Journal of Mechanics*, vol. 17, pp. 205-217.

**Zhu, J.; Zheng, L.; Zhang, X.** (2011): Hydrodynamic plane and axisymmetric slip stagnation-point flow with thermal radiation and temperature jump. *Journal of Mechanical Science and Technology*, vol. 25, no. 7, pp. 1837-1844.

**Zhu, J.; Zheng, L.; Zhang, Z. G.** (2010): Effects of slip condition on MHD stagnation-point flow over a power-law stretching sheet. *Applied Mathematics and Mechanics*, vol. 31, pp. 439-448.